Adhesion tilt-tolerance in bio-inspired mushroom-shaped adhesive microstructure

Lars Heepe, Giuseppe Carbone, Elena Pierro, Alexander E. Kovalev, and Stanislav N. Gorb
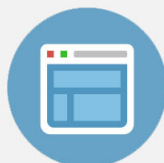
Adhesion tilt-tolerance in bio-inspired mushroom-shaped adhesive microstructure

Lars Heepe,[1] Giuseppe Carbone,[2] Elena Pierro,[3] Alexander E. Kovalev,[1] and Stanislav N. Gorb[1]

[1]*Functional Morphology and Biomechanics, Zoological Institute, Kiel University, Am Botanischen Garten 1-9, 24118 Kiel, Germany*
[2]*Tribolab - Dipartimento di Ingegneria Meccanica e Gestionale - Politecnico di Bari, V.le Japigia 182, 70126 Bari, Italy*
[3]*Scuola di Ingegneria, Università degli Studi della Basilicata, 85100 Potenza, Italy*

We studied experimentally and theoretically the effect of different tilt angles on the adhesion of mushroom-shaped adhesive microstructures. The marginal measured influence of tilting on pull-off forces is quantitatively well confirmed by numerical and theoretical calculations and was shown to be a direct consequence of an optimized stress distribution. In addition, the presence of a joint-like narrowing under the contact elements, as found in some biological attachment systems, was shown to further contribute to the tilt-tolerance. The results obtained allow us to explain the advantage of the widely observed mushroom-shaped contact geometry in nature for long-term and permanent adhesion. © 2014 AIP Publishing LLC. [http://dx.doi.org/10.1063/1.4860991]

In various biological adhesive systems, mainly two contact geometries have been evolved to serve the specific needs of attachment of organisms: spatula-shaped and mushroom-shaped contact geometry.[1] Spatula-shaped contact elements are mainly found in systems employing short-term adhesion used in fast locomotion (attachment-detachment cycles maximally for a few minutes) of, e.g., insects, spiders, and geckos.[1–5] Those contact elements show anisotropic, direction-dependent adhesion and have to be actively brought into contact.[2,4,6] Mushroom-shaped contact elements have been independently developed at the macro-, micro-, and nano-scale in the evolution of many organisms from different lineages (animals, plants, fungi, and bacteria) living in both terrestrial and aquatic environments.[1] This specific geometry is able to stay passively adhered without external effort and is mainly related to long-term and permanent adhesion of organisms.[1] Thus, one may assume that mushroom-shaped contact elements adhering to a substrate should be tolerant to changing and varying load conditions as, e.g., life in wave-swept seashores (e.g., sea anemones) and the long-term pairing process in some organisms.

Inspired by this geometry, many successful attempts were made to produce bio-inspired adhesives with arrays of individual mushroom-shaped contact elements.[7–11] Although adhesive and frictional properties were intensively studied,[7,9–14] only recently, the advantages of this contact geometry (compared to, e.g., flat punch geometry), regarding normal adhesion, were both theoretically and experimentally clarified.[15–18] However, in biological systems, the load conditions can strongly vary in different environmental and behavioural situations. That is why one may hypothesize that this particular contact geometry is not only optimized to normal adhesion but is also tolerant to the angle of applied pull off force.

In this Letter, we report on adhesion experiments aimed at testing the hypothesis that this contact geometry is tolerant to varying load conditions. Experiments have been carried out on individual mushroom-shaped adhesive microstructures (MSAMSs), see Fig. 1(a), pulled under different tilt angles. The resulting pull-off forces are compared to Finite Element (FE) calculations performed on the same geometry [Fig. 1(a)] and to approximate theoretical predictions of the influence of tilt angle on pull-off forces. Both experiments, numerical and theoretical calculations, are in good quantitative agreement.

In the experiments, four individual MSAMSs, denoted by samples **1–4**, were detached from a smooth glass slide under different tilt angles $\alpha = \{-45°, -10°, 0°, 10°, 45°\}$ simultaneously recording the failure dynamics. Individual MSAMSs were cut off from the tape made from polyvinylsiloxane (PVS) with a thickness of the supporting polymer film of about $900\,\mu m$.[8,14,17] Pull-off forces P_z [z direction only, see Fig. 1(b)] were measured using a force measuring system (FMS) consisting of a tensometric force transducers
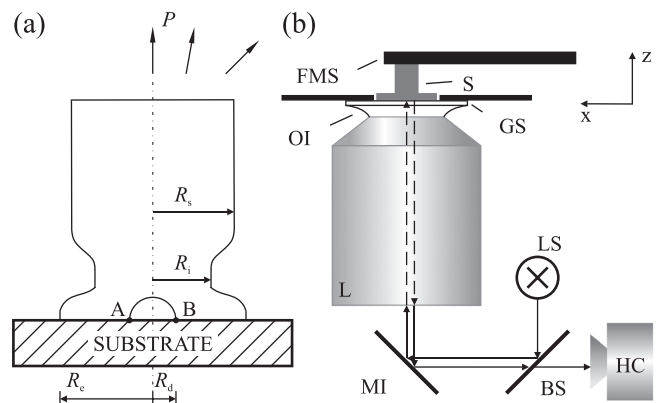

FIG. 1. (a) Geometry of an individual MSAMS used in the experiments and calculations with a circular area of radius R_d detached from the substrate at the center of the pillar. P, applied force at various tilt angles; R_i, internal neck radius; R_e, external thin contact plate radius; R_s, stalk radius. (b) Schematic of the experimental setup. FMS, force measuring system; S, sample; GS, glass slide; OI, oil immersion; L, lens; LS, light source; MI, mirror; BS, beam splitter; HC, high-speed camera.
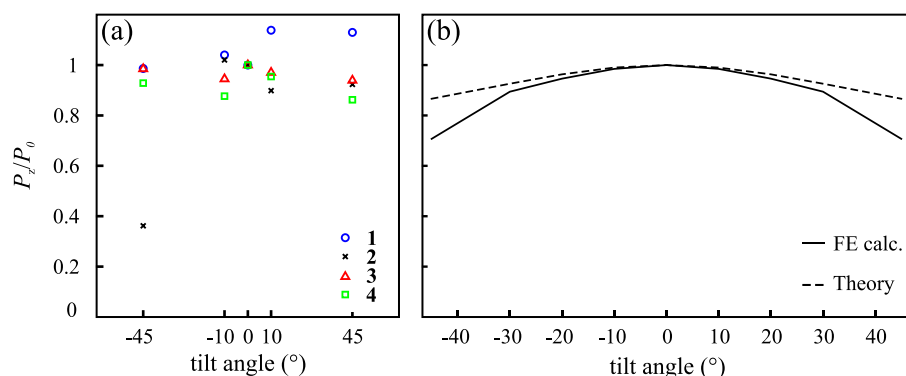
FIG. 2. (a) Normalized pull-off forces P_z/P_0 for different tilt angles α obtained from experiments. (b) Normalized pull-off forces obtained by FE calculations (solid line) and theoretical prediction (dashed line).

FORT-10 (World Precision Instruments, Inc., Sarasota, Florida) fixed on a three-axis micromanipulator F-131.3SS (Physik Instrumente GmbH & Co. KG, Karlsruhe, Germany). The FMS was installed on an inverse microscope Observer.A1 (Carl Zeiss MicroImaging GmbH, Göttingen, Germany) observing the detachment behavior with an attached high-speed camera Photron Fastcam SA1.1 (VKT Video Kommunikation GmbH, Pfullingen, Germany). Figure 1(b) shows the schematic of the experimental setup. In order to repeatedly attach and detach samples, individual MSAMSs were glued to the force transducer. To ensure parallel alignment between samples and the glass slide, individual MSAMSs were first attached to the glass slide manually using tweezers to observe the proper contact via the microscope. Then, attached to the glass slide, samples were withdrawn at a retraction velocity of $v_z = 10\,\mu$m/s normal to the glass slide (z direction). In order to pull under different tilt angles, a velocity $v_x = \pm v_z \tan \alpha$ in the x direction [see Fig. 1(b)] was superimposed on v_z. We remark that the retraction process occurred under displacement rather than load controlled conditions.

Figure 2(a) shows the experimentally obtained pull-off forces P_z for the different tilt angles α normalized by $P_0 \equiv P_z(\alpha = 0^\circ)$. Except for an outlier (sample **2**, $\alpha = -45^\circ$), normalized pull-off forces scatter surprisingly only by about $\pm 10\%$ around P_0 for all angles measured without certain trend.

We also carried out a FE analysis of an individual MSAMS [Fig. 1(a)] aimed at calculating the critical stress at which the MSAMS is pulled off from the substrate when a preexisting circular defect of radius R_d is located at the interface close to the pillar axis [Fig. 1(a)]. We have employed a mesh made of SOLID45 elements[19] with very high density in those regions where singular stress behavior is expected and observed, i.e., at the perimeter of the circular defect. A numerical value of the radius $R_d = 3\,\mu$m, in agreement with experimental observations,[17] has been used for calculations. The pull-off load and stress intensity factors $K^I = \lim_{r \to R_d} \sqrt{2\pi(r - R_d)}\ \sigma_{zz}(r, \theta)$, $K^{II} = \lim_{r \to R_d} \sqrt{2\pi(r - R_d)}\ \sigma_{zr}(r, \theta)$, and $K^{III} = \lim_{r \to R_d} \sqrt{2\pi(r - R_d)}\sigma_{z\theta}(r, \theta)$ [where r is the distance from the central axis of the pillar and θ is the in-plane angular coordinate] are calculated following the procedure described in Ref. 16. Observe that, this time, because of tilting [see Fig. 1(a)], K^I, K^{II}, and K^{III} are not uniform on the perimeter of the detached area [Figure 1(a)]. The most critical condition is, therefore, reached at point A in Fig. 1(a) where $K^{III} = 0$ and the equivalent stress intensity

factor is $K_{eq} = [(K^I)^2 + (K^{II})^2]^{1/2}$. In Fig. 2(b), we show the results of our FE simulations, in terms of normalized pull-off force P_z/P_0 (solid line), for different tilt angles of the external applied load, i.e., $\alpha = \{-45^\circ, -10^\circ, 0^\circ, 10^\circ, 45^\circ\}$.

Beside FE calculations, we have also used an approximate analytical approach to predict the pull-off force. To this end, first observe that, in absence of any defect, an optimized MSAMS presents an almost uniform normal stress distribution σ_{zz} in the central part of the contact[16] (i.e., the interfacial stress at the interface does not show any singular behaviour or any strong peak). However, because of tilting, additional stress components will appear at the interface, as tilting produces three types of stresses as shown in Fig. 3. Focusing only on the central part of the contact these stresses are: (i) the almost uniform normal stress σ_{zz}, (ii) the tangential stress σ_{zx}, and (iii) a triangular stress distribution σ_{zz}^T. Notice that if the defect is located relatively close to the center of the pillar, the triangular stress distribution σ_{zz}^T, caused by bending, is very negligible compared to σ_{zx} and σ_{zz}. Therefore, we expect that, in presence of a central defect, the dominant contribution to K_{eq} will come from stresses σ_{zz} and σ_{zx} only. We note that the stress σ_{zx} is, in
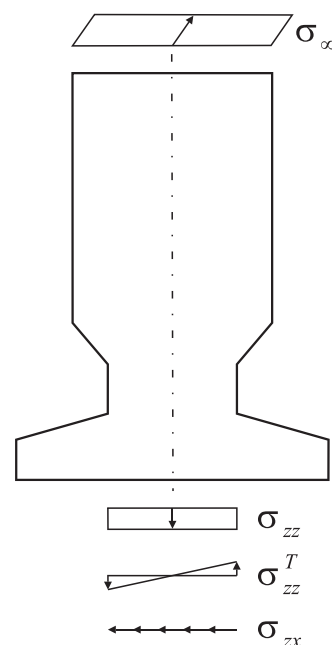

FIG. 3. The three types of stress distributions under the plate due to the external tilted load σ_∞ applied to the pillar: the uniform normal stress σ_{zz}, the tangential stress σ_{zx}, and the triangular stress distribution σ_{zz}^T.

general, not uniformly distributed at the interface; however, a rough estimation K^I and K^{II} will be done assuming a uniform distribution of σ_{zx}.

In this case, the pull-off force P_z can be estimated, observing that under tilted-load conditions the central defect resembles the case of a penny-shaped crack subjected to a linear combination of two remote loads: (i) a pure traction[20] and (ii) a pure shear load.[21] One can then use the superposition principle to combine the two stress states. Hence, the stress intensity factors, relevant for pull-off calculations, are: (i) $K_\perp = \max K^I$ related to the remote traction load, and (ii) $K_\parallel = \sqrt{(K^{II})^2 + (K^{III})^2}$ for shear mode. $K_\perp$ and $K_\parallel$ can be estimated as[20,21]

$$K_\perp = 2\sqrt{\frac{R_d}{\pi}}\sigma_T \cos^2\alpha, \qquad (1)$$

$$K_\parallel = \frac{2}{(2-\nu)}\sqrt{\frac{R_d}{\pi}}\sigma_T \sin(2\alpha), \qquad (2)$$

where ν is the Poisson's ratio, $\sigma_T = f\sigma_\infty$ is the equivalent remote total stress at the interface, $f \approx (R_s/R_i)^2 > 1$ is a factor that takes into account that σ_T and σ_∞ involves different areas [see Fig. 4] where R_s is the stalk radius of the pillar and R_i is the neck radius], and α is the tilting angle of the applied load. The accurate value of f has been calculated with the aid of FE analysis for $\alpha = 0°$. Incidentally, observe that $K_\parallel$ is uniform on the perimeter of the defect.[21] The equivalent stress intensity factor is in this case $K_{eq} = \sqrt{K_\perp^2 + K_\parallel^2}$ and enforcing the Griffith condition

$$G = \frac{K_{eq}^2}{2E^*} = \Delta\gamma \qquad (3)$$

allows the calculation of the z-component P_z of the pull-off force for different tilting angles α as

$$\frac{P_z}{P_0} = \sqrt{\left[\cos^4\alpha + \left(\frac{\sin 2\alpha}{2-\nu}\right)^2\right]^{-1}}\cos\alpha. \qquad (4)$$

Figure 2(b) (dashed curve) shows the results of Eq. (4) compared to FE predictions. We observe that for load tilting angles α ranging within $\pm 20°$ FE calculations and Eq. (4) are in very good agreement. However, the difference is no longer negligible at high load tilting angles, meaning that the effect of the two different assumptions (no slip for FE calculations and uniform frictional stress for analytical calculations) becomes relevant. Comparison with the experimental results shows that the analytical approach (Eq. (4)) is more effective than the FE model to capture the slight dependence of P_z on tilting.

We observe that the marginal influence of tilting on pull-off force, proved by experiments and numerical/theoretical calculations, is strictly a consequence of the optimal geometry of the pillar, which prevents the formation of singular stress distribution at the edge of the contact area, i.e., at the perimeter of the plate [Fig. 4(a)]. Indeed, non-optimal geometries as the one shown in Fig. 4(b) determine the occurrence of stress singularity at the edge of the plate, and cause the mushroom-shaped pillar to detach following the mode I behavior (i.e., crack propagation from the edge) as described in Ref. 15. This of course very significantly increases the sensitivity of pull-off force on tilting because the appearance of triangular normal stress distribution at the interface enhances the maximum value of the stress intensity factor at the perimeter of the plate.

Another important question concerns the effect of the neck on tolerance to tilting of mushroom shaped pillars. The neck strongly increases the bending compliance of the pillar, thus reducing the sensitiveness to force tilting. In fact, when an external tilted force is applied, a certain amount of bending will also occur (Fig. 5), leading to a reduction from α to α' of the angle between the applied force and pillar axis, i.e., to a reduction of the bending moment and, in turn, of the triangular stress distribution. For stiff pillars [e.g., without
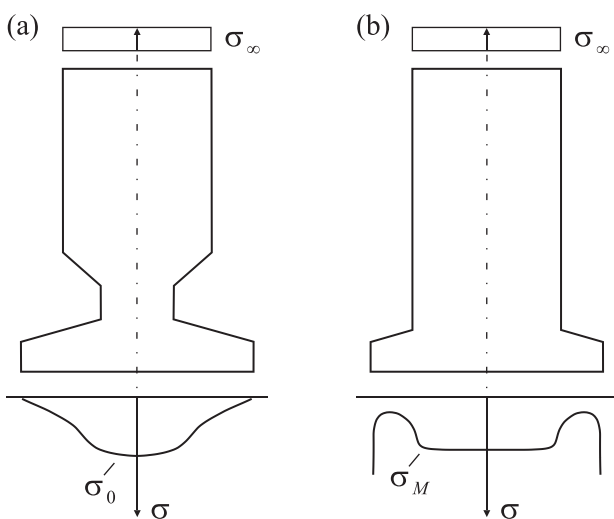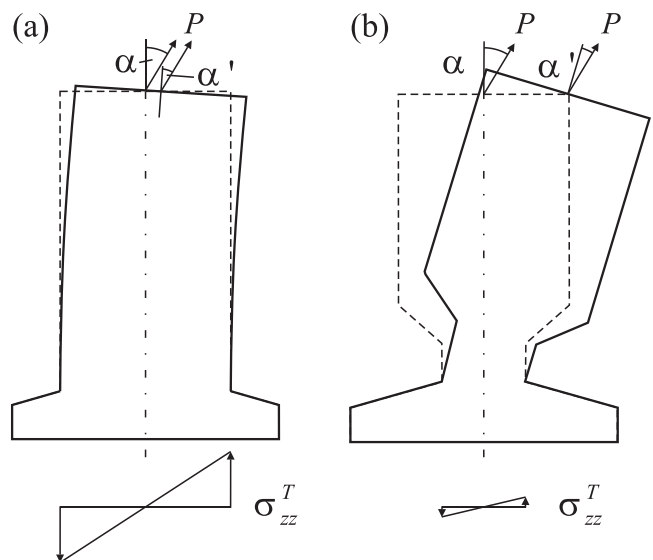

FIG. 4. The normal stress distribution σ_0 under the mushroom-shaped pillar with the neck and the normal stress distribution σ_M under the modified pillar.

FIG. 5. Triangular stress distribution σ_{zz}^T of a mushroom-shaped pillar without neck (a) and with neck (b) bended under a tilted force P.

neck Fig. 5(a)], the change $\Delta\alpha = \alpha - \alpha' \ll \alpha$ and a strongly detrimental triangular stress distribution will appear at the interface, which may significantly (even for optimized geometry) facilitate the pillar detachment. On the other hand, the presence of the neck [Fig. 5(b)] strongly reduces the stiffness and, in the limiting case of very high bending compliance, $\Delta\alpha = \alpha - \alpha' \approx \alpha$, i.e., $\alpha' = 0$, this causes an almost complete vanishing of the triangular stress distribution at the interface thus keeping the high values of pull-off force of mode II debonding mechanism.

So far, we have assumed a crack to appear in the center of the contact interface between MSAMS and the substrate. This assumption may not always hold in real experiments.[17] However, in light of above mentioned, a reduction of or a vanishing triangular stress distribution would also allow MSAMS with eccentric cracks to detach at the high values of pull-off force of mode II. Thus, the presence of a neck (or jointlike feature) provides tilt-tolerant adhesion also under experimental conditions.

Moreover, a neck may also offer further advantages. Structures with a neck not only provide tilt-tolerant detachment, but could also assist attachment. The reduced bending stiffness would allow for a better adaptability to uneven and non-parallel substrates compared to MSAMS without neck or a flat punch. In addition, recent experiments suggest that a neck makes MSAMSs also tolerant to high compressive loads. *In situ* scanning electron microscopy (SEM) observations of the contact behavior of MSAMSs indicated that the thin contact plate remained in contact, although MSAMS were buckled.[22] By contrast, flat punch pillars were shown to lose adhesive contact to the substrate at a critical load.[23]

It is interesting to note that some beetles of the family Chrysomelidae and calliphorid flies also have such jointlike feature between the stalk and the discoidal contact plate of their adhesive tarsal setae [Figs. 6(a) and 6(b)]. These setae as well as setae of other beetles[3] and earwigs[24] also contain an additional jointlike structure at the base of pillars. Such basal joints together with joints under the terminal contact elements are also known for suction cups of males of aquatic beetles[25] [Figs. 6(c) and 6(d)]. Joint-bearing plant hooks also demonstrate stronger tolerance to the tilting angle.[26]

In summary, we have examined both experimentally and theoretically the effect of tilted pull-off on the adhesion of individual MSAMSs. The experimentally obtained marginal effect is well confirmed by numerical and theoretical calculations and allows us to explain the advantage of the widely observed mushroom-shaped contact geometry in nature for long-term and permanent adhesion. The robustness or tilt-tolerance of MSAMS was shown to be a direct consequence of the optimized (homogeneous) stress distribution without singularities at the edge of the thin contact plate. Finally, the presence of a neck or jointlike feature between the stalk and the thin contact plate of mushroom-shaped contact elements was shown to further contribute to the robustness.
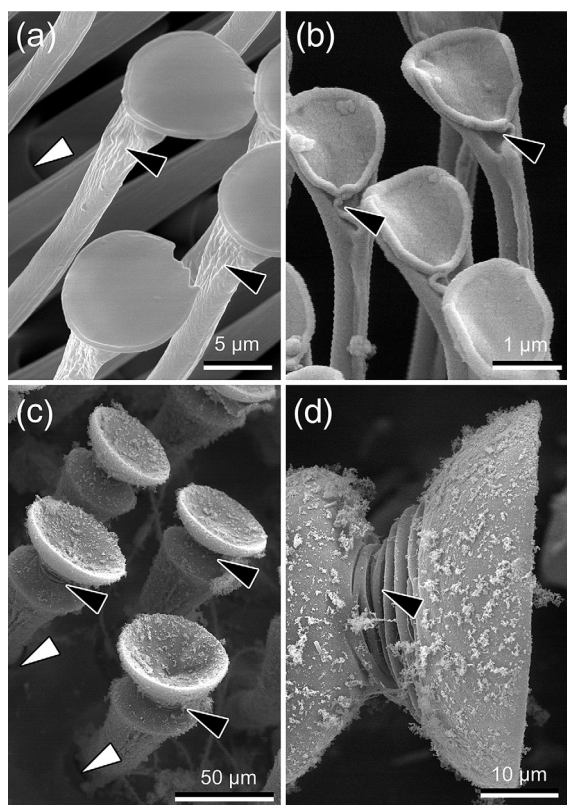
FIG. 6. Scanning electron microscopy images of insect tarsal adhesive microstructures with two types of microjoints: below the adhesive disc (black arrowheads) and at the base of the stalk/pillar (white arrowheads). (a) Adhesive setae of the chrysomelid beetle *Leptinotarsa decemlineata*; (b) Adhesive setae of the calliphorid fly *Calliphora vicina*; (c), (d) Microsuckers of the dytiscid beetle *Dytiscus marginalis*.

[1]S. N. Gorb and M. Varenberg, J. Adhes. Sci. Technol. **21**, 1175 (2007).
[2]K. Autumn, Y. Liang, S. Hsieh, W. Zesch, W. Chan, T. Kenny, R. Fearing, and R. Full, Nature **405**, 681 (2000).
[3]S. N. Gorb, *Attachment Devices of Insect Cuticle* (Springer, 2001).
[4]M. Varenberg, N. M. Pugno, and S. N. Gorb, Soft Matter **6**, 3269 (2010).
[5]S. N. Gorb, in *Handbook of Adhesion Technology*, edited by L. DaSilva, A. Ochsner, and R. Adams (Springer, Berlin, 2011), Vols. 1 and 2, pp. 1409–1436.
[6]A. Filippov, V. L. Popov, and S. N. Gorb, J. Theor. Biol. **276**, 126 (2011).
[7]S. Kim and M. Sitti, Appl. Phys. Lett. **89**, 261911 (2006).
[8]S. Gorb, M. Varenberg, A. Peressadko, and J. Tuma, J. R. Soc. Interface **4**, 271 (2007).
[9]A. del Campo, C. Greiner, and E. Arzt, Langmuir **23**, 10235 (2007).
[10]J. Davies, S. Haq, T. Hawke, and J. P. Sargent, Int. J. Adhes. Adhes. **29**, 380 (2009).
[11]D. Sameoto and C. Menon, J. Micromech. Microeng. **19**, 115002 (2009).
[12]S. Kim, B. Aksak, and M. Sitti, Appl. Phys. Lett. **91**, 221913 (2007).
[13]M. P. Murphy, B. Aksak, and M. Sitti, Small **5**, 170 (2009).
[14]L. Heepe, A. Kovalev, M. Varenberg, J. Tuma, and S. Gorb, Theor. Appl. Mech. Lett. **2**, 014008 (2012).
[15]G. Carbone, E. Pierro, and S. N. Gorb, Soft Matter **7**, 5545 (2011).
[16]G. Carbone and E. Pierro, Small **8**, 1449 (2012).
[17]L. Heepe, A. E. Kovalev, A. E. Filippov, and S. N. Gorb, Phys. Rev. Lett. **111**, 104301 (2013).
[18]L. Afferrante and G. Carbone, Macromol. React. Eng. **7**, 609–615 (2013).

[19]ANSYS User's Manual, Version 10.0, ANSYS, Inc.

[20]I. Sneddon, Proc. R. Soc. London A, Math Phys. Sci. **187**, 229 (1946).

[21]H. Tada, P. C. Paris, G. R. Irwin, and H. Tada, *The Stress Analysis of Cracks Handbook* (ASME Press, New York, 2000), Vol. 130.

[22]M. Varenberg and S. Gorb, J. R. Soc. Interface **5**, 785 (2008).

[23]D. Paretkar, M. Kamperman, A. S. Schneider, D. Martina, C. Creton, and E. Arzt, Mater. Sci. Eng., C **31**, 1152 (2011).

[24]F. Haas and S. Gorb, Arthropod Struct. Dev. **33**, 45 (2004).

[25]K. K. Green, A. Kovalev, E. I. Svensson, and S. N. Gorb, J. R. Soc. Interface **10**, 20130409 (2013).

[26]E. Gorb, V. Popov, and S. Gorb, Des. Nature **57**, 151 (2002).